Proceedings of the 35th International Conference on Ocean, Offshore and Arctic Engineering
OMAE2016
June 19-24, 2016, Busan, Korea

OMAE2016-54435

REAL-TIME HYBRID MODEL TESTING OF A BRACELESS SEMI-SUBMERSIBLE WIND TURBINE. PART I: THE HYBRID APPROACH

Thomas Sauder*
MARINTEK
7450 Trondheim, Norway
NTNU AMOS / IMT
7491 Trondheim, Norway

Valentin Chabaud
NTNU / IMT
7491 Trondheim, Norway

Maxime Thys
MARINTEK
7450 Trondheim, Norway

Erin E. Bachynski
MARINTEK
7450 Trondheim, Norway

Lars Ove Sæther
MARINTEK
7450 Trondheim, Norway

ABSTRACT

This article presents a method for performing Real-Time Hybrid Model testing (ReaTHM testing) of a floating wind turbine (FWT). The advantage of this method compared to the physical modelling of the wind in an ocean basin, is that it solves the Froude-Reynolds scaling conflict, which is a key issue in FWT testing. ReaTHM testing allows for more accurate testing also in transient conditions, or degraded conditions, which are not feasible yet with physical wind. The originality of the presented method lies in the fact that all aerodynamic load components of importance for the structure were identified and applied on the physical model, while in previous similar projects, only the aerodynamic thrust force was applied on the physical model. The way of applying the loads is also new. The article starts with a short review (mostly references) of ReaTHM testing when applied to other fields than marine technology. It then describes the design of the hybrid setup, its qualification, and discusses possible error sources and their quantification. The second part of the article [1] focuses on the performance of a braceless semi-submersible FWT, tested with the developed method. The third part [2] describes how the experimental data was used to calibrate a numerical model of the FWT.

1 INTRODUCTION

Despite the rise of increasingly sophisticated numerical models and tools, physical hydrodynamic model testing in a controlled environment is still required for verifying new designs of offshore structures. Some complex physical phenomena are indeed still not fully understood, nor modelled numerically. Example of such phenomena are extreme wave loads (slamming, ringing, and green-water on deck), viscous loads (roll and yaw damping of ship-shaped floaters, or viscous effects limiting gap resonance in side-by-side configurations), or wave-current interaction effects on floating moored structures. On the other hand, model testing also has limitations, depending strongly on the application. When testing floating wind turbines (FWT), important issues are limitations of laboratory infrastructure in terms of wind generation equipment, scaling effects and the incompatibility between scaling laws.

The concept of *Real-Time Hybrid Model Testing* (or ReaTHM^{TM} testing, a trademark of MARINTEK) has its origin in (1) these experimental limitations, combined with (2) the improvement of theoretical/numerical models' fidelity, and with (3) increases in available computational power. In ReaTHM testing, one part of the system is modelled physically, while the

*Corresponding author (thomas.sauder@marintek.sintef.no)

other part, whose behaviour is assumed to be well described theoretically, is modelled numerically. Both physical and numerical substructures interact, in real-time, through a network of sensors and actuators. ReaTHM testing is used in general to study complex systems when (1) the limitations on the physical size or characteristics of testing facilities do not allow a full model of the system to be accommodated, (2) when conflict in scaling between different subsystems hinders the use of conventional model testing, and (3) when the focus of the test is the performance of a single module or component in a complex system. In the latter case, ReaTHM testing allows simplifying the setup for a more effective execution of the tests, or to reduce uncertainties from the other modules.

Objective The main objective of the present article is to describe how this technique was newly applied to achieve accurate aerodynamic loading on a floating wind turbine. In this case, aerodynamic/generator loading was evaluated numerically, and all load components of importance were applied in real-time onto the physical substructure located in MARINTEK's Ocean Basin. Wave loads were physical, so Froude scaling was applied. Wind loads were numerical, evaluated in full-scale and scaled down using Froude scaling. This guaranteed a consistent scaling of the problem, and a controlled incoming wind field. The method is illustrated by a case study involving the braceless semi-submersible 5MW-CSC wind turbine [3], tested at 1:30 scale. Note that *a key prerequisite of the presented method is the validity of the numerical tools used for the evaluation of the aerodynamic loads*. This aspect is not the focus of the present work. It is however briefly discussed in Section 6, and it is the object of detailed study in other projects [4].

Outline Section 2 gives a brief review of ReaTHM testing in fields where this technique is considered as mature. Section 3 describes the overall methodology and architecture of the ReaTHM test setup employed for testing of a FWT. In Section 4, the focus is on the procedure applied to verify and qualify the hybrid system. For completeness, Section 5 briefly lists the types of investigations that ReaTHM testing enables in the field of wind engineering. For a complete case study, the reader is referred to Part II [1], which shows in particular that this technique enabled accurate investigation of the coupled responses of the FWT and its controller. Unique test conditions, such as blade pitch fault situations and shutdown, could also be investigated. Finally, Section 6 of the present article discusses error sources, and suggests ways to quantify and mitigate them.

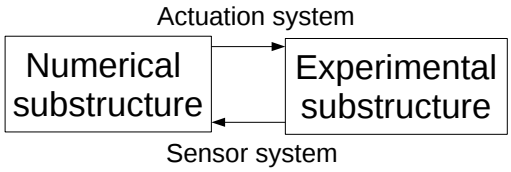

FIGURE 1. Principle of Real-time Hybrid Model Testing.

2 HYBRID TESTING: CONCEPT AND APPLICATIONS

ReaTHM testing refers to the method in which a physical system under study is partitioned into at least two *substructures*: a *physical substructure* tested experimentally in model-scale, connected to a *numerical substructure* simulated on a computer. The two parts interact with each other in real-time through a network of sensors and actuators. See Figure 1.

Background ReaTHM testing has its roots in the field of earthquake engineering. Interfacing experiments with simultaneous simulations to study the structural behaviour of large scale buildings was envisioned in the 1970's in Japan [5]. The idea progressed and became a standard tool for studying damage-mitigating components for buildings or bridges. The United States [6] and Europe [7] also have active communities focusing on the development and use of this method. In the field of automotive engineering, similar ideas have been applied to simulate aerodynamic forces on sports cars [8], or to test individual parts, such as gearboxes, in industrial automotive developments [9, 10, 11]. The development of ReaTHM testing required an unprecedented interaction between the various disciplines of numerical and experimental methods, signal processing and control engineering. Each discipline was also individually challenged by some new requirements, which led to interesting developments: new classes of numerical methods were for instance developed that proved superior to classical (e.g. Runge-Kutta) methods in terms of stability and efficiency for stiff problems [12]. Novel finite element formulations for slender structures were developed, with a special treatment of axial properties that allowed real-time dynamic simulations of cables [13]. New error quantification criteria were developed that could be calculated *online*, i.e. during the execution of a ReaTHM test [14, 15]. In addition to those examples of fundamental developments, advanced methods, such as model-based control strategies [5], or stability analyses based on Delayed Differential Equations [16] were applied to new types of problems. In the field of marine technology, few ReaTHM tests have been reported; see [17, 18] and references therein. ReaTHM testing has been identified as a promising technology for testing of FWTs. The review in Part II [1] provides details on this issue, its importance, and the various solutions that have been suggested by others [19, 20].

Nomenclature ReaTHM testing techniques have been developed and used in various fields, quite independently from each other. This led to various nomenclatures, which may be misleading when looking for references. The terms "real-time hybrid testing" or "real-time hybrid simulations" are common in earthquake engineering [5, 21], "real-time dynamic substructuring" seems more in use in mechanical engineering [10] , while the terms "hardware-", "software-", or "model-in-the-loop" tend to be preferred by others [8, 20]. The denomination of "substructure", however, seems quite common across these fields, to describe the various elements, either numerical or physical, of the substructural partition. Note that this is not to be mixed with the term "substructure" used in offshore technology, which refers to a foundation. When applying this method to the field of marine technology, the terminology "real-time hybrid model testing" was preferred by the authors, since i) it shows a natural connection to classical hydrodynamic "model testing", ii) the terms "real-time" and "model" emphasize the fact that the processing and calculations involved should run in *Froude-scaled real-time*.

3 DESIGN AND DEVELOPMENT OF THE HYBRID SETUP

Designing a ReaTHM test of floating wind turbine involved a number of tasks, which can be summarized by the following steps:

1. Define the *quantities of interest*, i.e. the quantities of importance for the designer, which should be investigated through testing. In our case, those quantities were the (rigid body) motions of the platform, the tensions in the mooring lines, and the structural loads at the tower/floater interface and at the joint between one side column and the pontoon.
2. Define the *frequencies of interest*, i.e. the frequency range on which the quantities of interest have to be captured correctly by the tests. In the present case study, flexible modes of the FWT, such as the bending modes of the tower, were out of the scope of the investigation[1]. The frequency content of the quantities of interest was therefore determined by the bandwidth of the rigid prototype, and the frequency and amplitude of the environmental loads. Figure 2 summarizes the frequency map of the problem. Even though the highest eigenfrequency of the FWT was well below the wave spectrum peak frequency, waves include a significant amount of energy, and corresponding frequencies were therefore expected to have a significant effect on the quantities of interest, especially due to aerodynamic damping. It was therefore decided that the frequencies of interest were $[0, 2]$ Hz, in model scale 1:30.

[1]Flexible modes could be of importance for other designs, as TLPs, in which the coupling between the (higher-frequency) floater motions and the flexible modes are more significant.

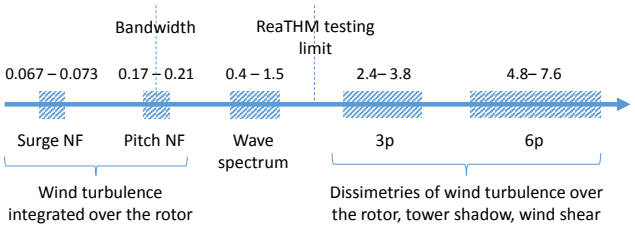

FIGURE 2. Frequency map. Frequency values are in Hz, model scale. p denotes the rotational speed of the rotor. NF denotes natural frequency.

3. Choose a *substructuring strategy*, i.e decide which component of the system will be numerical, and which one will be physical.
4. Perform a *sensitivity analysis to limited actuation*. In principle, the six components of the load vector evaluated by the numerical model should be applied to the physical substructure. However, in order to reduce the complexity of the setup while ensuring adequate fidelity, it is worth considering whether some components of the load vector can be removed without significantly affecting the quantities of interest.
5. When the load pattern from the numerical substructure to the physical substructure has been estimated, define the *actuator placement and the allocation strategy*.
6. Design and tune the *control system*, including the required instrumentation
7. Proceed to the *verification* tests.

In Subsections 3.1 and 3.2, steps (3)-(5) will be detailed using the 5-MW-CSC wind turbine as a case study. Subsection 3.3 will provide the main ideas behind step (6). Step (7) will be treated in Section 4.

3.1 Substructuring strategy

Figure 3 shows the substructural partition, in which components that should be Froude-scaled are separated from those that should in principle be Reynolds-scaled. The *physical substructure* included the semi-submersible of the 5-MW-CSC design [3], and the tower design described in [22]. Details regarding the geometry and mass properties of the physical substructure are given in Part II [1]. The *numerical substructure* included all components of the wind turbine mounted on the top of the tower. Note however that the mass of the numerical substructure was included in the physical substructure, in order to include rigid-body inertial loads in a simple yet accurate way (gyroscopic moments will be discussed below). The wind turbine in the numerical substructure was the NREL 5MW wind

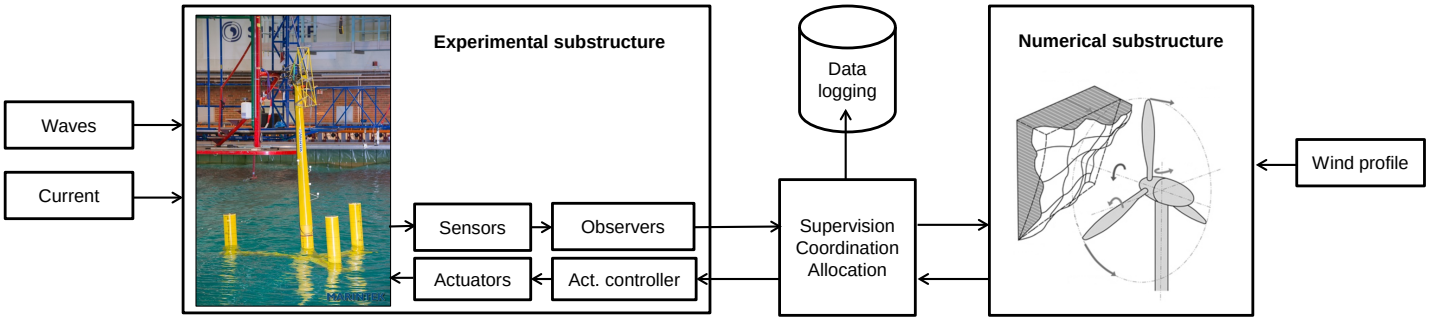

FIGURE 3. Substructuring strategy. The numerical substructure contains only the turbine (its mass is modelled physically, though) while the floater and rigid tower are modelled physically. Wave and current environment are modelled physically in the Ocean Basin, while the wind environment is modelled numerically.

turbine [23]. Its blades were assumed rigid, and 17 elements were applied along each 63m long blade. The element distribution was largely dictated by the blade geometry. The generator torque was determined based on the Bladed-style DISCON controller defined for the OC3 study [23]. The controller used proportional-integral control with gain scheduling for collective blade pitch, and a lookup table for generator torque. The controller was modified for cases where blade pitch fault or shutdown were to be included.

Environmental loads While the surface waves and ocean currents were modelled physically, the oncoming turbulent wind was modelled numerically using time series generated in TurbSim v1.5 [24]. A mesh of 28x28 elements covering a surface of 160x160m was used. Detailed properties regarding the incoming wind field are given in Part II [1]. The aerodynamic load calculations were carried out in full-scale using the open source code AeroDyn [25]. AeroDyn is a well-known implementation of the blade element/momentum (BEM) and generalized dynamic wake (GDW) methods. The wind loads were scaled down using Froude-scaling before being applied on the turbine. Figure 4 summarizes the procedure.

Choice of the time steps Available computational power set a lower bound on the step size in both AeroDyn and TurbSim, and memory limitations an upper bound on the mesh fineness on the blades and the wind field. However, the time-steps used in AeroDyn and TurbSim should be consistent with each other. NREL recommends using a step size of 20ms in AeroDyn [25], with a default value set to 25ms for the NREL 5MW model. In the present work, based on a priori estimation of required computational power, the numerical models were run at 100Hz, which corresponds to a step size of 55ms in full-scale. The increase in time step in the aerodynamic solver has a limited impact on

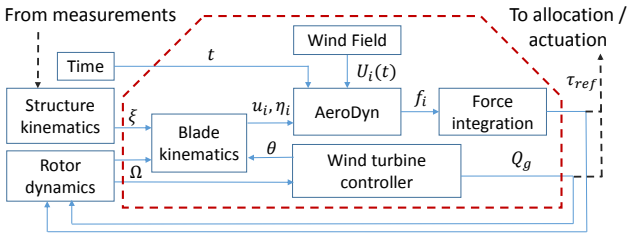

FIGURE 4. Block diagram of the numerical substructure including AeroDyn, the wind turbine controller, the pre-defined wind field, kinematic and integration routines. The quantities inside the dashed red box are in full-scale while the others are in model scale.

the integrated loads at the frequencies of interest: as the loads are applied in an integrated manner, some error in modelling the local aerodynamic forces on individual blade elements is acceptable. On the other hand, the step size recommended by NREL for TurbSim is 50ms [24]. TurbSim uses this value as a basis for its Nyquist frequency (the highest turbulence frequency is half of the inverse of the time step size). To avoid aliasing, the time step used in TurbSim must therefore be at least equal to the time step used in AeroDyn (NREL recommends a factor of two). In the present study, memory limitations of the selected hardware appeared to be dominating, and TurbSim's time step size was therefore set to 22ms. It was verified numerically that this had no effect on the rigid-body response of the FWT[2], and that the selected time steps and spatial mesh resolutions were therefore consistent with each other and with the problem at hand.

[2]Coherence links the size of the vortices with their frequency. High frequency variations, linked to small variations in space, are cancelled out when averaged over a large area. Therefore, if not seeking for local (elastic) effects, the step size may be safely increased. For the same reason, a coarser sampling in time allows a coarser sampling in space.

3.2 Sensitivity to limited actuation and actuator placement.

Aerodynamic loads from the numerical substructure should be applied to the physical substructure using one or several actuators. The number, the type and the location of those actuators with respect to the physical substructure must be determined [19]. Ideally, a technical arrangement could have been developed, that could apply *any* given load vector to the physical substructure, with obviously some upper and lower bounds. However, since some components of the aerodynamic load were known to be smaller than others, it could have been tempting to assume that the corresponding load effects were also smaller, which would have allowed reducing the requirements on the setup. The "BCS method", described in [26], allowed an informed decision to be made.

Briefly, the BCS method consists in running integrated analyses of the FWT in tools like SIMA [27], removing one by one the components of the aerodynamic loading, and studying the consequence on the quantities of interest, defined at the beginning of this Section. The conclusion drawn after this study [26] was that *five out of the six components of the aerodynamic loading significantly affected the quantities of interest* and should therefore be included in the ReaTHM test. In addition to the vertical aerodynamic force, it was found that the inertial loads induced by the rotation of the turbine (the so-called gyroscopic moments) could be neglected. Note however that this conclusion was valid for a given floater and a given wind turbine design, and as importantly, for a given test matrix. The conclusion would most probably be different when changing those parameters.

Let $\tau = [T, F_y, Q_g, M_y, M_z] \in \mathbb{R}^5$ be the load vector from the numerical substructure to the physical substructure. T is the thrust force, F_y the horizontal tangential aerodynamic force, Q_g the generator torque, and M_y and M_z the pitch and yaw aerodynamic moments at the rotor, respectively. The arrangement that was chosen to apply the load is presented in Figure 5. A square frame was mounted at the nacelle location. A minimal set of six actuators with pulleys were fixed alongside the Ocean Basin, and connected to the frame using thin lines. A pretension F_0 was added lines 1 to 4 to avoid slack. Let $F \in \mathbb{R}^6$ be the vector containing the magnitude of the forces from each actuator. Augmenting τ with the pretension, the problem was fully actuated in a workspace of dimension 6, with a Jacobian $J \in \mathbb{R}^{6\times6}$ satisfying:

$$\tau = J(\eta)F \tag{1}$$

$J(\eta)$ is a nonlinear function of the position and attitude $\eta \in \mathbb{R}^6$ of the physical substructure, and of the position of the actuators. A pseudo-inverse of $J(\eta)$ can be computed, mapping exactly the desired loads τ_{ref} to the commanded tensions F_{ref}.

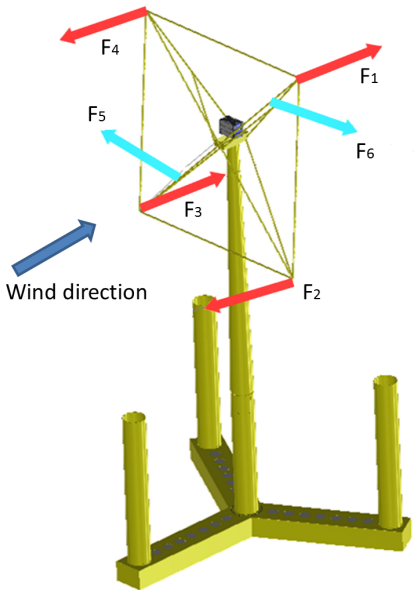

FIGURE 5. Illustration of the physical substructure, and of the top frame on which the load vector τ is applied. The forces F_i from each actuator are also represented. Note that for clarity, the frame is represented with a larger dimension than in reality. Additional pretension was used on the lines represented by red arrows.

TABLE 1. Main contribution from each actuator force F_i (see Figure 5) to the components of the load vector τ, and to the pretension F_0

	T	F_y	Q_g	M_y	M_z	F_0
F_1	X			X		X
F_2				X	X	X
F_3	X				X	X
F_4						X
F_5		X	X			
F_6		X	X			

Table 1 shows the main contribution from each of the lines to the load vector, obtained from the first-order Taylor expansion of $J(\eta)^{-1}$. This can easily be related to the physical setup shown in Figure 5.

3.3 Control system and instrumentation

An overall block diagram including the physical and numerical substructures, the sensor system and the actuation system is presented in Figure 6. The numerical substructure, detailed in Figure 4, received the kinematical data of the physical substructure as an input. The positions, orientations, and

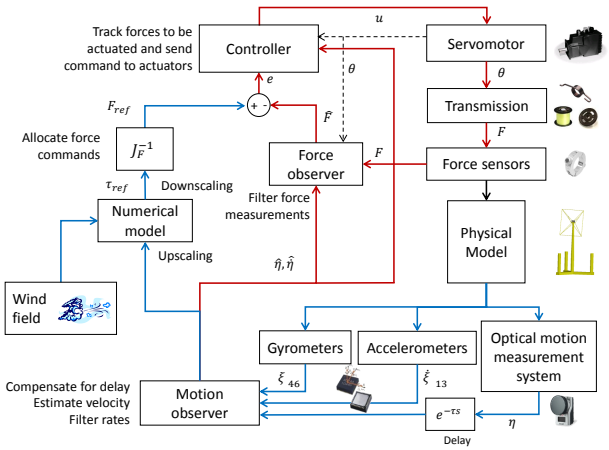

FIGURE 6. Overall block diagram of the control system.

velocities, of the blade elements were computed based on the actual rotor speed and hub position, and passed to AeroDyn. The rotor speed was computed based on its inertia, on the generator torque, and on the aerodynamic torque. The hub position in the wind field was obtained based on the measured position and attitude of the physical substructure. Once the numerical model returned the aerodynamic/generator loads τ_{ref} to be applied on the physical model, the allocation procedure discussed earlier was applied to generate the reference line force vector F_{ref}. The red lines in Figure 6 represent the inner actuation loop running at a higher frequency that ensured the force control function. Both feed-forward and feedback force control were used [17]. The former made use of the measured motions of the physical substructure, while the latter made use of measurements from force rings mounted between the actuator lines and the square frame on the physical model. Zero-order hold of the forces was applied.

The sensor system for evaluating the motions of the physical substructure consisted in three types of sensors: an optical measurement system, gyrometers, and accelerometers. The OQUS optical measurement system provided the position and attitude of the FWT at a frequency of 100Hz. The corresponding acquisition system was however running asynchronously, involved some computational time, and the signals were transmitted through a non-real-time network, so measurements were received with a delay. This delay was identified as almost constant from preliminary tests, and compensated for by using polynomial interpolation/extrapolation [5]. Angular velocities from the gyrometers were sampled at 600Hz and filtered with a Butterworth low-pass filter of order 3 with a cut-off frequency of 5 Hz, in order to remove spurious structural vibrations of the physical substructure. The linear velocities were derived at 600Hz by an observer making use of accelerometer signals (which are prone to drift), and positions/attitude from the optical position measurement system (which were available at 100Hz only). It was verified that the velocity predicted by the observer matched with the differentiated position from the OQUS system transformed into the body-fixed coordinate system.

The data from the numerical substructure (such as the rotor speed and the pitch angle of the blades) and physical substructure (motions, and structural loads) were logged in a synchronized way. For traceability, all data specific to the hybrid setup (such as the commanded force F_{ref} or the measured forces F_m) were also logged. Several dedicated quantities were also logged in order to quantify delays in the control loop.

3.4 Virtual testing with SIMA

Prior to connecting any actuator to the controller, it was verified that the commanded loads, calculated based on the physical substructure's motions and environmental excitation, were correct. To do so, MARINTEK's simulation platform SIMA [27] played the role of the physical substructure in Figure 3, following the classical "Hardware-in-the-Loop" approach when testing e.g. DP systems [28]. The physical substructure, actuators and the connection lines were modelled in SIMA, and the simulated position and velocity of the structure were sent as an input to the controller. This test allowed detecting potential errors in the allocation procedure outlined in Section 3, improving safety procedures, and running sensitivity studies on the time step used in the numerical model, among others.

4 VERIFICATION OF THE HYBRID SETUP

As in classical model testing, a qualification of the test setup was required, before executing the planned test matrix with the 5MW-CSC turbine. The various verification steps that were performed are detailed in the following subsections.

4.1 Following mode and disturbance rejection

Running ReaTHM testing in *following mode* means that the commanded load vector τ_{ref} from the numerical substructure onto the physical substructure is prescribed to zero[3]. Note that the actuator lines are still connected to the physical substructure, with pretension. With the control system in this mode, the physical substructure was subjected to two types of disturbances: motions induced by the systems' own dynamics (decay tests), and motions induced by wave excitation. The same tests were then repeated, but with the actuators disconnected. The quantities of interest (motions, mooring line tensions, and

[3]Note that $F_{i,d} = 0$ was used instead of $\tau_{ref} = 0$ during these tests, which is not equivalent due to the presence of pre-tension in the lines. This induced a minor error, negligible in the case of the surge decay.

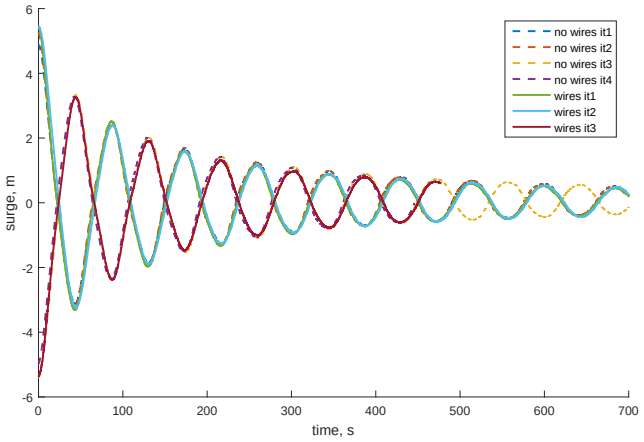

FIGURE 7. Surge decay test, without wind. Four decays were performed without actuators (dashed lines), two starting with a positive surge excursion, and two with a negative initial excursion. Similarly, three decay tests were performed with the hybrid system connected, and working in following mode (solid lines).

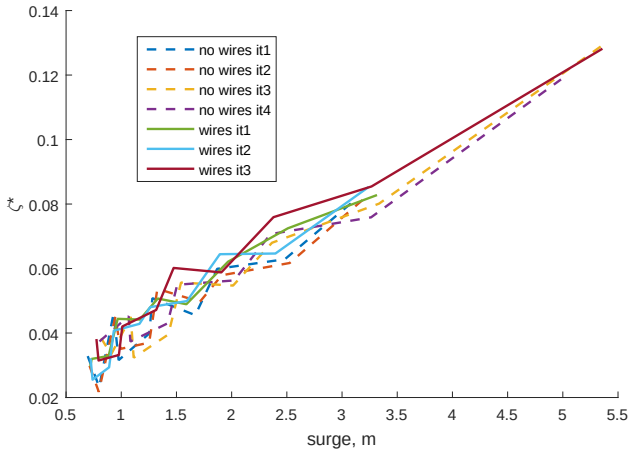

FIGURE 8. Damping ratio as a function of the surge amplitude. Same conditions as in Figure 7. $\zeta^* = \frac{1}{\sqrt{1+\left(\frac{2\pi}{\delta}\right)}}$, where δ is the logarithmic decrement.

structural loads) were then compared to evaluate the disturbance rejection capacity of the control system.

Decays in all six degrees of freedom were performed: first without the hybrid system, and then with the system in following mode. Decay tests in following mode are an efficient way of checking whether the hybrid setup modifies the eigenperiods, or introduces spurious damping or excitation in the system. It was checked that the eigenperiods with ReaTHM in following mode were within a few percent of those of the free structure. Figure 7 shows time series of decay in surge. For this mode of motion, the eigenperiod was identified equal to 86.49s when the actuators were disconnected, and was 0.4% lower during ReaTHM testing in following mode. The damping ratio ζ^* as a function of the surge amplitude was evaluated from those time series, and shown in Figure 8. The lowest eigenperiod of the structure under study was 25.4s (heave motion), which was much larger than the targeted bandwidth of our control system. Higher frequency excitation was achieved using regular and irregular waves. No other load than the wave loads were applied during these tests. Table 2 compares their mean values and standard deviations during the irregular wave test. The deviation between the two tests was generally below 6%, which was found acceptable.

4.2 Time-varying load tracking

Once the disturbance rejection capacity of the system was checked, the focus was on verifying its capacity to track a time-varying reference $\tau_{ref}(t)$. To do so, a (numerical) turbulent wind profile was generated, and the corresponding aerodynamic/generator loads were applied onto the physical substructure. Note that the motions of the physical substructure induced a relative wind velocity at the nacelle, which influenced the loading on the numerical substructure. This influence is one of the main reasons for pursuing this type of tests, and should therefore be accurately captured.

TABLE 2. Standard deviations of the quantities of interest during irregular wave tests (H_s=3.6m, T_p=10.2s) with actuators disconnected, or connected but in following mode. Deviation in percent.

Quantity	Disconnected	Following mode	
Surge [m]	0.43	0.44	+2.8%
Heave [m]	0.21	0.22	+2.7%
Pitch [deg]	0.23	0.23	-1.9%
Bending moments [MNm]			
- side column	7.70	7.85	+1.9%
- tower base	5.94	6.26	+5.4%
Mooring line tension 1 [kN]	18.10	18.01	-0.5%
Mooring line tension 2 [kN]	18.77	19.85	+5.7%
Mooring line tension 3 [kN]	28.68	29.59	+3.2%

Repeatability Repeatability of the tests in turbulent wind was the first focus. Table 3 shows statistics of the quantities of interest during two successive tests, and Figure 9 shows a random window of the time series of the surge and pitch motions as well as the bending moment. Comparing mean values and standard deviations, we see that repeatability is excellent, except for the measured heave standard deviation which is impaired by measurement inaccuracies (model-scale motions are of the order of 2mm, which is close to the resolution of the optical motion measurement system). It was also verified that the repeatability was

TABLE 3. Repeatability tests. Standard deviations of the quantities of interest during turbulent wind test 11m/s (numerical wind only, no physical waves or current).

Quantity	Test 1	Test 2	Deviation
Surge mean [m]	-7.89	-7.95	+0.7%
Surge std. dev. [m]	1.66	1.66	-0.5%
Heave std. dev. [m]	0.06	0.08	-
Pitch mean [deg]	5.76	5.73	-1.9%
Pitch std. dev. [deg]	1.17	1.18	+0.9%
Bending moments [MNm]			
- side column, mean	-8.82	-8.80	+0.2%
- side column, std. dev.	2.38	2.40	+0.8%
- tower base, mean	85.29	84.73	-0.7%
- tower base, std. dev.	14.01	14.19	+1.3%
Mooring line tension [kN]			
- Line 1, mean	1828	1830	+0.1%
- Line 1, std. dev.	64.7	64.8	+0.2%
- Line 2, mean	1820	1825	+0.3%
- Line 2, std. dev.	63.1	62.5	-0.9%
- Line 3, mean	1165	1163	-0.2%
- Line 3, std. dev.	68.0	67.7	-0.4%

excellent during combined wind and wave tests.

Comparison between desired and applied loads The focus was then on showing that the measured load vector τ_m adequately followed the command τ_{ref} sent by the numerical model. The incoming wind velocity was chosen near the rated wind speed of 11 m/s: the aerodynamic thrust force was then at its maximum value, and the use of both blade pitch and generator torque controllers was triggered; see for instance the sudden variation of Q_g in Figure 10. The same, reasonably rough, sea-state was considered as in Table 2. The actually actuated force tensor $\tau_m(t)$ was computed from the measured forces $F(t)$ and measured physical substructure motions η_m, by means of equation (1). It was compared to the commanded tensor $\tau_{ref}(t)$. Results are plotted in Figure 10.

The actuation accuracy of the thrust force, generator torque and pitch and yaw moments was very satisfactory at low frequencies where most of the wind excitation and eigenfrequencies lie. This was valid up to about 2 Hz model scale, i.e. for the whole range of frequencies of interest. It means the aerodynamic damping to wave excitation was also properly actuated. However higher frequencies were dramatically amplified. These frequencies were outside the range of frequencies of interest, and would only be relevant if elastic modes of the structure were to be studied, which was out of the scope of this investigation. The tangential force F_y may seem poorly actuated. However, the standard deviation of F_y was 0.25 N model scale, which is beyond the targeted accuracy of the actuators, and this inaccuracy was expected to have a negligible effect on the response.

A comparison of the time series of the actuated load components was also included in Figure 10. A frequency domain

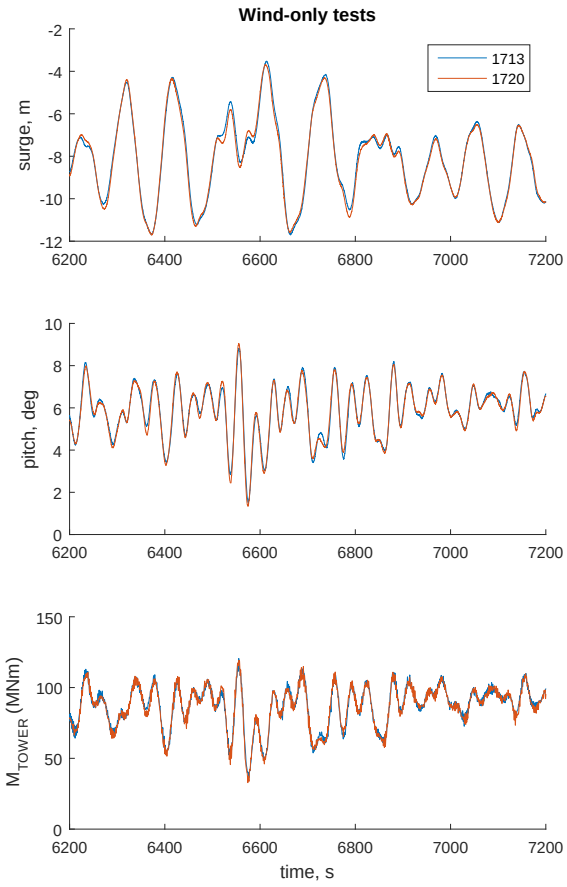

FIGURE 9. Repeatability-check of wind-only loading. Randomly selected time window and time-series of surge and pitch motions, as well as bending moment at the tower base.

comparison is indeed not enough to assess the performance of the load tracking. While a phase shift between desired and actuated loads would lead to fairly similar power spectral densities of the components of τ, they would differ from each other through the effect the phase shift has on the response, when fed back into the numerical model.

5 CAPABILITIES OF THE HYBRID SYSTEM FOR FWT

Once well-functioning, the setup allowed the following tests to be performed. (1) Decay tests in wind velocities below, above and at the rated speed of the generator. (2) Tests in combined wind, waves and current, including regular and irregular waves, misaligned wind and waves, and extreme wave conditions. (3) Tests were also carried out to examine the transient dynamics of the FWT under fault conditions, which, to the authors knowledge, has not been studied experimentally before. Two scenarios

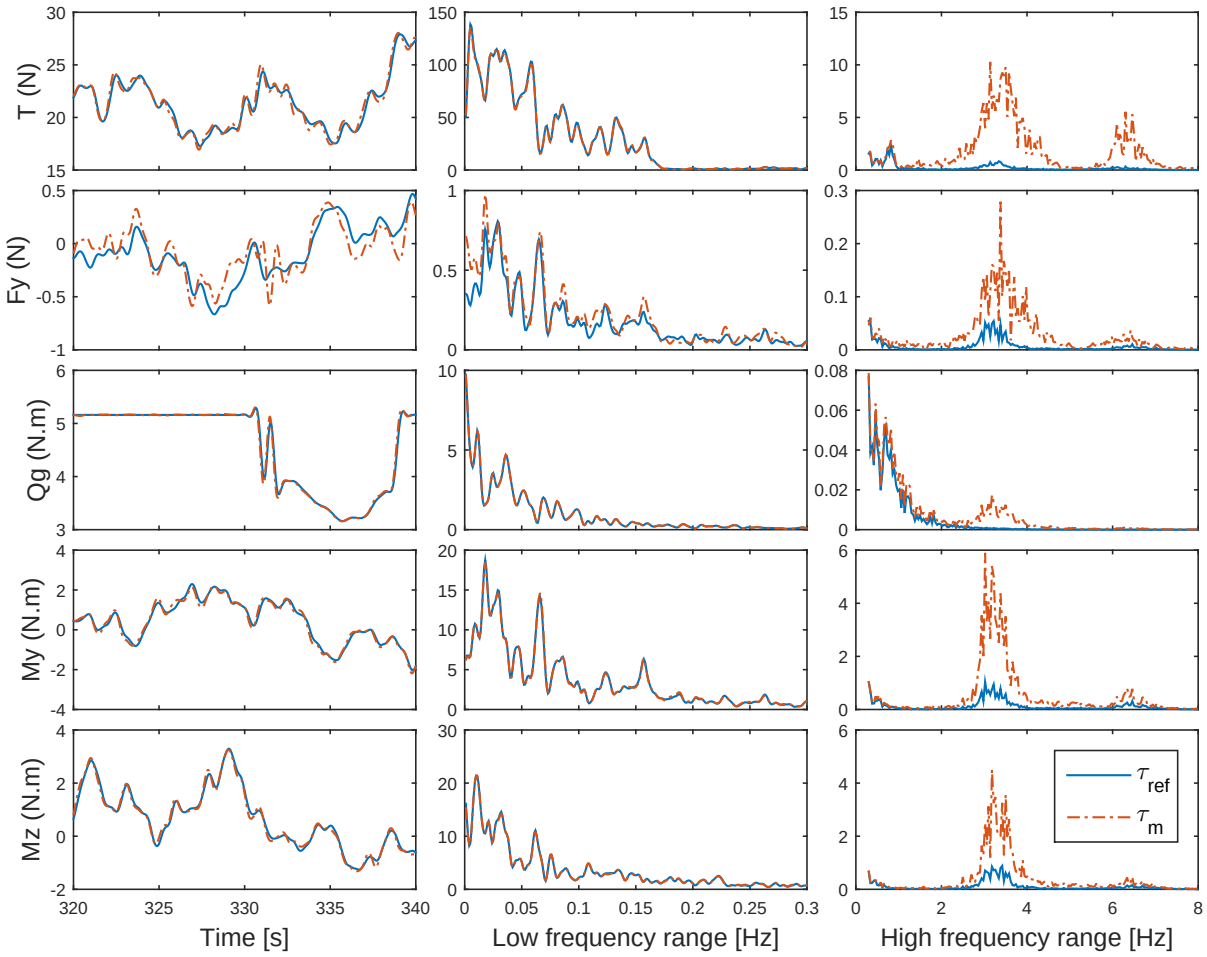

FIGURE 10. Desired and measured rotor loads τ_{ref} and τ_m, respectively. The plots on the left-hand side show a time-series window filtered at 2 Hz (upper bound of the frequency range of interest). Spectra for low frequency loads (from wind excitation integrated over the 3 blades, and the natural frequencies of the substructure) are shown at the center. Spectra of the high frequency loads (from wave excitation, and rotational sampling of turbulence by each individual blade) are shown on the right-hand side. Frequency values are in model scale (1:30).

were investigated: emergency shutdown of the generator in large wind speeds, and blade seize (one blade loses the ability to pitch). Transient motions of FWT, transient loads on the mooring lines and at the tower base could be studied, as well as the dynamics of the FWT in shutdown or degraded mode. Selected results of (1)-(3) are reported in detail in [1]. Even if not tested during the present test campaign, the developed methodology enables (4) testing generators and rotors from various manufacturers on the same substructure in a quite efficient way, (5) testing various control strategies for the wind turbine controller, without necessarily disclosing the details of the controller, and (6) performing detailed sensitivity studies to the wind modelling (including effect of large waves on the wind field).

6 ERROR SOURCES AND MITIGATION

The very goal of ReaTHM testing of FWT is to provide more accurate estimates of the quantities of interests than when testing using classical methods, involving physical aerodynamic modeling. Sections 3 and 4 outlined the incremental design and verification procedures, which were required by the fact that ReaTHM testing is a more complex operation than "classical" testing. Experimental errors are usually separated in the two following categories. *Random errors* come from unknown or unpredictable

events happening during the tests, as sensor noise, data packet losses, or varying actuator performance due to change of its temperature. They can be quantified by repeating the tests as done in Section 4.2. *Systematic errors* are predictable, reproducible, and can be eliminated by modifying the ReaTHM test setup itself. In the following, it is attempted to list all possible sources of systematic errors, and propose ways of quantifying their influence on the accuracy of the results. The ambition of ReaTHM testing should be to demonstrate a level of accuracy comparable to professional wave tank testing of ships and offshore structures.

Imperfection of the physical substructure This aspect has received much attention in the past. See for instance [29] and references herein. Errors are mainly due to imperfections of the geometry or mass distribution of the physical model of the semi-submersible, and deviations from the specified wave and current environment. MARINTEK has procedures for controlling those aspects, which were applied during this test. Once uncertainties related to the physical substructure dynamics are quantified, methods exist to evaluate their consequence on the coupled system. See for instance [30].

Imperfections in the numerical model Even if ReaTHM testing allows for a *controlled* aerodynamic loading on FWT, the degree of fidelity of the numerical aerodynamic load modelling is still questionable. (1) In the present work, the incoming turbulent wind field has been generated by using TurbSim [24], which is mostly based on standards as IEC 61400-3 and current knowledge. However uncertainties remain, mainly due to the lack of full-scale data. As an example, the influence of waves on the marine atmospheric boundary layer, usually neglected, has been recently shown to be of importance when analyzing FWTs [31]. (2) For a given wind field, the evaluation of aerodynamic loading is made using AeroDyn. A validation study of the loads predicted by AeroDyn has given satisfactory results for fixed land-based wind turbines [32], and dedicated wind tunnel validation tests for moving towers are currently being performed [4]. (3) Our AeroDyn model assumed rigid blades. Consistently, the tower influence, generating impulse loads at a the triple of the rotor rotation frequency, and inducing blade vibrations, was neglected. Also, few elements were used along the blade. These choices were made *a priori* in order to simplify as much as possible the aerodynamic calculations and ensure a computation time compatible with the requirements outlined in Section 3. A posteriori, it was noticed that the model could have been running with more elements and a modal description of the blades without exceeding time constraints. Finally, (4) the time steps used in AeroDyn and TurbSim were above recommended values, even though they were consistent with the objective of the test. This was discussed in Section 3.1.

Delayed input to the numerical substructure In order to provide valid results, the numerical substructure must be correctly implemented and used with the proper settings (this was discussed in the previous paragraph), but it should also be provided with correct inputs. These are, in addition to the wind field provided by TurbSim,

1. The three linear velocities at the hub from the accelerometers and the optical position measurement system.
2. The three angular velocities of the structure from the gyrometers.
3. The position and attitude of the hub from the optical position measurement system, including time delay compensation.

Point 3 is assumed accurate: as discussed in 3.3, it is a key input to the force-tracking controller, and the performance observed in Figure 10 could not be achieved with erroneous or slightly delayed position/attitude. Linear accelerations and angular velocities were however directly derived from online measurements (without delay compensation) and their acquisition, processing and transfer induced a time delay. An upper bound of this time delay was found from dedicated measurements to be h =20ms. This corresponds to a phase delay $\phi(\omega) = h\omega$. An estimate of the consequence of such a delay on the properties of the system under study can be obtained through the following simplified analysis.

Assuming no coupling between the degrees-of-freedom of the structure, we focus on the aerodynamic damping, and assume that it is proportional to the body-fixed velocity of the structure (valid for small body velocities). Assuming no dynamic effect from the rotor wake and wave radiation, the motions of the FWT can be described by a set of uncoupled second-order harmonic oscillators with external forcing $u = A_u \sin(\omega t + \psi)$, induced for instance by waves.

$$\ddot{x} + 2\zeta\omega_n\dot{x} + \omega_n^2 x = u$$

ζ is the damping ratio consisting of both hydrodynamic and aerodynamic damping: $\zeta = \zeta_h + \zeta_a$. Denoting the harmonic surge or pitch response $x = A_x \sin(\omega t)$, we modify the aerodynamic damping, computing it from a delayed velocity. The equation becomes:

$$(\omega_n^2 - \omega^2)\sin\omega t + 2\omega_n\omega\left[\zeta_h\cos\omega t + \zeta_a\cos(\omega t - \phi)\right] = \frac{u}{A_x}$$

Since $\cos(\omega t - \phi) = \cos\omega t\cos\phi + \sin\omega t\sin\phi$, the "imperfect" aerodynamic damping ratio can be estimated as $\zeta_{a_d} = \zeta_a\cos\phi(\omega)$, and $\omega_{n_d}^2(\omega) = \omega_n^2 + 2\zeta_a\omega_n\omega\sin\phi(\omega)$.

Table 4 shows the effect of the delay on the aerodynamic pitch damping (which is different from the thrust-induced pitch damping). The phase angle used in the calculation was obtained

TABLE 4. Estimation of the effect of filtering and time delay - Aerodynamic pitch moment.

	Phase delay	Aerodynamic damping coeff.	Total restoring coeff.
Peak wave frequency	17 deg	-4.4 %	+1.7%
Pitch natural frequency	5 deg	-0.4 %	+0.1%

TABLE 5. Estimation of the effect of filtering and time delay - Aerodynamic thrust.

	Phase delay	Aero. damping coeff.	Total restoring coeff. Surge	Total restoring coeff. Pitch	Pitch response (α)
Peak wave frequency	4^o	-0.2%	+9.1%	+9.0%	+0.7%
Pitch natural frequency	1^o	-0.02%	+0.6%	+0.6%	+0.05%

from the properties of the filter used on the gyrometers (see Section 3.3). Both the error on the aerodynamic pitch damping coefficient and on the natural frequency were found acceptable. The effect of a delayed yaw rate on the yaw aerodynamic moment was similar to that of the pitch. It should be noted that the filter's cut-off frequency was chosen as low as 5 Hz due to spurious vibrations of the physical model that needed to be filtered. With an improved mechanical design, the filter cut-off frequency could be increased, and the filter-induced phase angles would decrease.

The imperfection in the gain of the transfer function of the system can be expressed as:

$$\alpha = \frac{\left|H_{u\to x}\left(\omega_{n_d},\zeta_d,\omega\right)\right| - \left|H_{u\to x}\left(\omega_n,\zeta,\omega\right)\right|}{\left|H_{u\to x}\left(\omega_n,\zeta,\omega\right)\right|} \tag{2}$$

where

$$\left|H_{u\to x}\left(\omega_n,\zeta,\omega\right)\right| = \frac{1}{\sqrt{\left(\omega_n^2-\omega^2\right)^2+\zeta\omega_n^2\omega^2}} \tag{3}$$

The quantity α was used to obtain estimates of the effect of the delay on the response of the system. The effect of time delay on the aerodynamic thrust is shown in Table 5. The effect on restoring in pitch was derived using the squared distance from the hub to the center of gravity. Surprisingly, even though the phase delay was lower, the effect on the restoring coefficient was larger than that estimated with the delayed pitch moment discussed above. Indeed the thrust force provides much more damping in pitch than the aerodynamic pitch moment, and even a small value of the phase delay can have a significant effect at the wave frequency. As mentioned in Section 4, the pitch eigenfrequency was practically unchanged since the change in restoring coefficient was only 0.6 % at the pitch natural frequency. The effect on the response was estimated by mean of Equation (2), and shown on the last column of Table 5. It was found acceptable. Note that the numerous assumptions that led to this simplified assessment method forbid any strict quantitative error evaluation, but rather a way of showing the consistency of the method.

Other structured uncertainties and controller performance The control system uses as an input a set of parameters describing the physical arrangement of the setup. Those include, but are not limited to, the properties of the actuators, of the transfer system (including the six lines), and of the attachment points of the lines on the physical substructure. Uncertainties regarding those parameters exist, which may compromise the force control. In the present work, procedures were developed and run several times during the tests for identifying and verifying model parameters, but no form of robust or adaptive control was applied. Comparing the time series of τ_{ref} and τ_m allowed quantification of the accuracy of the force tracking *a posteriori*. Another important aspect is related to time-delays induced by numerical computation, communication, and to some extent actuator response. Those will typically introduce spurious energy in the system, and may cause instabilities [16]. Our delay compensation strategy was based on kinematic predictors, which assumed a *constant* delay between the measured position and the applied force. This delay was determined from a priori tests. It was checked, for instance using the decay tests outlined in Section 4 that the delay was correctly compensated for, and did not cause any spurious variation of energy of the system.

Choices made to reduce the workspace In order to limit the number of actuators, we simplified the setup, deliberately neglecting some load components from the numerical substructure (the gyroscopic moments, and vertical aerodynamic loads). The consequence of this choice on the quantities of interest has been documented with the BCS method [26] and found acceptable.

Unstructured uncertainties Examples of such uncertainties include (but are not limited to) unmodelled dynamics, as vibrations of the load transfer system or of the square frame, random time delays, induced by hardware/software issues or network overload, or varying actuator performance, due to e.g. temperature. It is difficult to classify those uncertainties as "random" or "systematic" since they could be avoided by an improved design, but are not necessarily repeatable, which means that their non-occurrence can not be guaranteed through repeatability tests as reported in Section 4. Two strategies may be applied to detect them. The first one is to measure these delays and ensure their statistical properties remain below a critical limit. See for instance [33] regarding the stability of networked-controlled sys-

tems. Another solution is to monitor the *effects* of such uncertainties using energy criteria at the interface between the numerical and physical substructure as suggested in [34, 35, 15]. Such criteria have not been used in the present project, and remain to be developed for the present application.

7 CONCLUSION

A method for performing ReaTHM^{TM} testing of a floating wind turbine has been developed. Its originality lies in the fact that it (1) alleviates the Froude-Reynolds scaling conflict inherent to this problem, (2) includes all aerodynamic load components of importance for the structure, and (3) enables performing new type of tests, as turbine shutdown or blade seize scenarios. The goal of this new method was to increase the level of accuracy of FWT model testing in combined wind, waves and current, and hereby ensure safe and optimized FWT designs. A case study has been performed, during which the performance of the hybrid setup was scrutinized and verified. Possible error sources were discussed. Their quantification, as well as the qualification of the method for other types of offshore wind turbines, will be an important part of the upcoming research activities. The next part of this article [1] uses the developed testing method to focus on relevant physical properties of the 5MW-CSC design.

ACKNOWLEDGMENT

The authors gratefully acknowledge the financial support from the Research Council of Norway granted through the Norwegian Research Center for Offshore Wind Technology (NOWITECH), and from MARINTEK internal funding.

REFERENCES

[1] Bachynski, E. E., Thys, M., Chabaud, V., and Sauder, T., 2016. "Real-time Hybrid Model Testing of a Braceless Semi-submersible Wind turbine. Part II: Experimental Results". In 35th International Conference on Ocean, Offshore and Arctic Engineering, no OMAE2016-54437.

[2] Berthelsen, P. A., Bachynski, E. E., Karimirad, M., and Thys, M., 2016. "Real-time Hybrid Model testing of a Braceless Semi-submersible Wind turbine. Part III: Calibration of a Numerical Model". In 35th International Conference on Ocean, Offshore and Arctic Engineering, no OMAE2016-54640.

[3] Luan, C., Gao, Z., and Moan, T., 2016. "Design and analysis of a braceless steel 5MW semi-submersible wind turbine". In Proc. of 35th OMAE conf.

[4] MARINTEK, 2015. www.lifes50plus.eu - LIFES50+ - Innovative floating offshore wind energy.

[5] Carrion, J. E., 2007. *Model-based strategies for real-time hybrid testing*. ProQuest, Jan.

[6] Shao, X., and Griffith, C., 2013. "An overview of hybrid simulation implementations in NEES projects". *Engineering Structures,* ***56***, Nov., pp. 1439–1451.

[7] Pinto, A., Pegon, P., Magonette, G., and Tsionis, G., 2004. "Pseudo-dynamic testing of bridges using non-linear substructuring". *Earthquake Engineering & Structural Dynamics,* ***33***.

[8] Plummer, A. R., 2006. "Model-in-the-Loop Testing". *Proceedings of the Institution of Mechanical Engineers, Part I: Journal of Systems and Control Engineering,* ***220***(3), Jan., pp. 183–199.

[9] De Klerk, D., 2009. *Dynamic response characterization of complex systems through operational identification and dynamic substructuring: an application to gear noise propagation in the automotive industry.* [s.n.], [S.l.].

[10] De Klerk, D., Rixen, D. J., and Voormeeren, S. N., 2008. "General Framework for Dynamic Substructuring: History, Review and Classification of Techniques". *AIAA Journal,* ***46***(5), May, pp. 1169–1181.

[11] Li, G., 2014. "A generic dynamically substructured system framework and its dual counterparts". In World Congress, Vol. 19, pp. 10101–10106.

[12] Bursi, O. S., 2009. Monolithic and partitioned L-Stable Rosenbrock methods for dynamic substructure tests.

[13] Johansen, V., 2007. "Modelling of flexible slender systems for real-time simulation and control applications". PhD thesis, Norwegian University of Science and Technology.

[14] Mosqueda, G., Bozidar Stojadinovic, and Stephen A. Mahin, 2007. "Real-Time Error Monitoring for Hybrid Simulation. Part I: Methodology and Experimental Verification". *Journal of Structural Engineering,* ***133***(8).

[15] Maghareh, A., Dyke, S. J., Prakash, A., and Bunting, G. B., 2014. "Establishing a predictive performance indicator for real-time hybrid simulation". *Earthquake Engineering & Structural Dynamics,* ***43***(15), Dec., pp. 2299–2318.

[16] Kyrychko, Y., Blyuss, K., Gonzalez-Buelga, A., Hogan, S., and Wagg, D., 2006. "Real-time dynamic substructuring in a coupled oscillator–pendulum system". *Proceedings of the Royal Society A: Mathematical, Physical and Engineering Sciences,* ***462***(2068), Apr., pp. 1271–1294.

[17] Chabaud, V., Steen, S., and Skjetne, R., 2013. "Real-Time Hybrid Testing for Marine Structures: Challenges and Strategies". In ASME 2013 32nd International Conference on Ocean, Offshore and Arctic Engineering, American Society of Mechanical Engineers.

[18] Cao, Y., and Tahchiev, G., 2013. "A Study on an Active Hybrid Decomposed Mooring System for Model Testing in Ocean Basin for Offshore Platforms". In ASME 2013 32nd International Conference on Ocean, Offshore and Arctic Engineering, American Society of Mechanical Engineers.

[19] Hall, M., Moreno, J., and Thiagarajan, K., 2014. "Performance Specifications for Real-Time Hybrid Testing of 1: 50-Scale Floating Wind Turbine Models". In ASME 2014 33rd International Conference on Ocean, Offshore and Arctic Engineering, American Society of Mechanical Engineers.

[20] Azcona, J., Bouchotrouch, F., González, M., Garciandía, J., Munduate, X., Kelberlau, F., and Nygaard, T. A., 2014. "Aerodynamic Thrust Modelling in Wave Tank Tests of Offshore Floating Wind Turbines Using a Ducted Fan". *Journal of Physics: Conference Series,* ***524***, June, p. 012089.

[21] Nakata, N., Dyke, S. J., Zhang, J., Mosqueda, G., Shao, X., Mahmoud, H., Hite Head, M., Bletzinger, M., Marshall, G. A., Ou, G., and Song, C., 2014. "Hybrid Simulation Primer and Dictionary".

[22] Jonkman, J. M., 2010. *Definition of the Floating System for Phase IV of OC3*. National Renewable Energy Laboratory Golden, CO, USA.

[23] Jonkman, J. M., 2007. *Dynamics modeling and loads analysis of an offshore floating wind turbine*. ProQuest.

[24] Jonkman, B., 2009. TurbSim User's Guide. Version 1.50. Tech. rep.

[25] Moriarty, P. J., and Hansen, A. C., 2005. *AeroDyn theory manual*. National Renewable Energy Laboratory Golden, Colorado, USA.

[26] Bachynski, E. E., Chabaud, V., and Sauder, T., 2015. "Real-time Hybrid Model Testing of Floating Wind Turbines: Sensitivity to Limited Actuation". *Energy Procedia,* ***80***, pp. 2–12.

[27] MARINTEK, 2015. SIMA 3.2 User Guide. Tech. rep.

[28] Fossen, T. I., 2002. *Marine control systems: guidance, navigation and control of ships, rigs and underwater vehicles*, 3. printing ed. Marine Cybernetics, Trondheim.

[29] Qiu, W., Sales Junior, J., Lee, D., Lie, H., Magarovskii, V., Mikami, T., Rousset, J.-M., Sphaier, S., Tao, L., and Wang, X., 2014. "Uncertainties related to predictions of loads and responses for ocean and offshore structures". *Ocean Engineering,* ***86***, Aug., pp. 58–67.

[30] De Klerk, D., and Voormeeren, S., 2008. "Uncertainty propagation in ex-

perimental dynamic substructuring". In Proceedings of the Twenty Sixth International Modal Analysis Conference, Orlando, FL.

[31] Kalvig, S. M., 2014. "On wave-wind interactions and implications for offshore wind turbines".

[32] Laino, D., Hansen, A., Minnema, W., and Lake, S., 2002. "Validation of the AeroDyn subroutines using NREL unsteady aerodynamics experiment data". *Wind Energy,* ***5***, pp. 227–244.

[33] Hespanha, J. P., Naghshtabrizi, P., and Xu, Y., 2007. "A survey of recent results in networked control systems". *PROCEEDINGS-IEEE,* ***95***(1), p. 138.

[34] Ahmadizadeh, M., and Mosqueda, G., 2009. "Online energy-based error indicator for the assessment of numerical and experimental errors in a hybrid simulation". *Engineering Structures,* ***31***(9), Sept., pp. 1987–1996.

[35] Chen, C., and Ricles, J. M., 2010. "Tracking Error-Based Servohydraulic Actuator Adaptive Compensation for Real-Time Hybrid Simulation". *Journal of Structural Engineering,* ***136***(4).